Removal of lead ions from water by capacitive deionization electrode materials derived from chicken feathers

T. Alfredy, Y. A. C. Jande and T. Pogrebnaya

ABSTRACT

Capacitive deionization (CDI) is a promising and rapidly growing technology for water treatment and the electrode materials play a key role in improving CDI performance. In this study, high surface area activated carbon was prepared from chicken feather (CF) bio-waste through pyrolysis and KOH activation; the KOH:CF ratio (R) and activation temperature (T_a) were variable parameters. The material was characterized by using the Brunauer, Emmett and Teller (BET) method, Fourier transform infrared (FTIR) spectroscopy and scanning electron microscopy (SEM). The lead (Pb^{2+}) removal test was performed with a CDI cell containing the fabricated carbon electrode and 100 mg L^{-1} $Pb(NO_3)_2$ solution; the sample prepared with the ratio R of 1:1 and $T_a = 800$ °C exhibited higher Pb^{2+} removal efficiency of 81% and electro sorption capacity of 4.1 mg g^{-1} at the electrode potential 1.2 V and flow rate 5 mL min^{-1}. Therefore, CF-derived carbon is considered as a promising CDI electrode material for removal of heavy metals from waste water.

Key words | activated carbons, batch mode, capacitive deionization, chicken feathers, heavy metal, lead removal

T. Alfredy
Y. A. C. Jande (corresponding author)
T. Pogrebnaya
Department of Materials and Energy Science and Engineering,
The Nelson Mandela African Institution of Science and Technology,
P.O. Box 447, Arusha,
Tanzania
E-mail: *yusufu.jande@nm-aist.ac.tz*

Y. A. C. Jande
Water Infrastructure and Sustainable Energy Futures Centre of Excellence,
The Nelson Mandela African Institution of Science and Technology,
P.O. Box 9124, Nelson Mandela, Arusha,
Tanzania

INTRODUCTION

Currently, water pollution is a growing challenge worldwide due to the increase in human activities such as agriculture, industries and mining, which continuously generate toxic heavy metals (Mdegela *et al.* 2009). Among the toxic heavy metals, lead (Pb^{2+}) has been categorized as a serious hazardous due to its effect on the human body. This metal can damage the human kidney, liver, brain, nervous, and reproductive systems (de la Rosa *et al.* 2008). Therefore, the removal of this metal from water is a focal point of recent research. To date, several technologies such as reverse osmosis, membrane filtration, chemical precipitation, ion exchange resins, and distillation have been used (Huang *et al.* 2016). Despite the fact that each method has a number of advantages, they have some limitations. For instance, reverse osmosis and thermal processes are considered for large-scale water desalination but their commercial application requires high initial cost, a large workforce, and high energy consumption (Porada *et al.* 2012; Huang *et al.* 2016; Chen *et al.* 2017a, 2017b). Therefore, new desalination methods are required to overcome these challenges. Capacitive deionization (CDI) is a promising and rapidly growing technology that is easy to operate, environmentally friendly and energy efficient for brackish water (<10,000 mg L^{-1}) purification (Suss *et al.* 2015). It is reported to consume 0.4 kWh m^{-3}, for total dissolved solids (TDS) removal for brackish water desalination (Jande 2015; Peng *et al.* 2016).

doi: 10.2166/wrd.2019.074

Water desalination by CDI is based on the principle of the electric double layer capacitors (EDLCs), where the charged ions such as Pb^{2+} and NO_3^- can be adsorbed from the aqueous solution and electrostatically stored on the oppositely charged electrode surfaces (anode and cathode) through the application of voltage from an external power source (Baroud & Giannelis 2018). Once the external voltage is removed, the trapped ions can be released back to the solution, which results in regeneration of the electrodes. Chemical and physical properties of materials used for the electrodes play vital roles in the capacitive behavior.

To date, a wide range of materials such as porous carbon, carbon aerogel, activated carbon cloth, nitrogen-doped carbon materials, graphene, nanostructured carbon cloth, nanoporous silicon dioxide or alumina surface doped with magnesium, carbon nanotubes and nanofibers have been used as electrode materials in CDI applications (Peng *et al.* 2016; Li *et al.* 2017). Though carbon aerogel and graphene met most of the specifications required for CDI applications, their practical application is hindered by their high cost (Machunda *et al.* 2009). Therefore more studies focusing on the development of renewable and low-cost electrode materials for CDI applications are needed (Lado *et al.* 2016). Currently, various biomass wastes such as coffee residue, sugarcane bagasse, wood, coconut shells, rice husks, and chicken feathers have attracted many types of research. These materials provide an alternative source for carbon precursor since they can be synthesized at very low cost, and possess high surface area, good electrical conductivity and suitable pore size distribution (Wang *et al.* 2013; Yang *et al.* 2015; Zhao *et al.* 2015; Lado *et al.* 2016).

Approximately 24 billion chickens are slaughtered worldwide each year which entails disposing of 1.8×10^9 kg of feather waste. The huge amount of waste produced is either dumped directly to the environment causing soil and groundwater source pollution or openly burnt to pollute the air causing health effects to humans (Prasanthi *et al.* 2016). Thus, studies were done to convert the feather waste into materials for various commercial applications such as adsorbents for water treatment (de la Rosa *et al.* 2008) and electrode materials for EDLCs (Wang *et al.* 2013; Zhao *et al.* 2015). To the best of our knowledge, there have been no reported studies on the use of chicken feathers (CF) for CDI applications. Therefore, this study aims to evaluate chicken feathers as a potential material for CDI electrodes, in particular for the removal of Pb^{2+} from the water.

MATERIALS AND METHODS

Materials

Chicken feathers were collected from Kilombero poultry market in Arusha region, Tanzania. The chemicals including potassium hydroxide (KOH), lead nitrate ($Pb(NO_3)_2$), ethanol and hydrochloric acid (HCl) were of analytical reagent grade, polytetrafluoroethylene (PTFE, 60 wt % dispersion in H_2O) and carbon black were purchased from Sigma Aldrich. All chemicals were used without any modification.

Preparation of chicken feather activated carbon

Chicken feathers were washed thoroughly with distilled water and then dried at 90 °C for 12 h in the oven, ground to powder and carbonized in a horizontal tube furnace (CTF 12/65/550) at 400 °C for 1 h at a heating ramp rate of 5 °C min^{-1} in the presence of nitrogen. The carbonized carbon char was chemically activated by KOH in the weight ratio KOH to carbon (KOH:CF) of 1:1, 2:1, 3:1 and 4:1 at 600 °C, 700 °C and 800 °C under nitrogen flow for 3 h at a heating rate of 5 °C min^{-1}. The tube furnace was allowed to cool naturally at room temperature before activated products were removed. The samples were washed with 1 M HCl to remove KOH and with hot distilled water to remove the residual KCl until neutral pH was attained, and finally dried in an oven at 100 °C for 12 h. The material produced was denoted as CF and CF-R-T_a-t, representing the chicken feather carbon and activated carbon derived from chicken feathers, respectively. The letters R, T_a, and t represent KOH to carbon mass ratio, activation temperature and activation time (in hours), respectively. On the other hand, the untreated carbon was labeled as CF-400, where 400 denotes carbonization temperature.

Characterization of materials

The textural properties of the prepared CF samples, Brunauer, Emmett and Teller (BET) surface area, pore diameter and pore size distribution, were obtained from

physical N_2 adsorption-desorption isotherm measurements at liquid nitrogen temperature 77 K by a surface area and porosity analyzer (Quantachrome NovaWin ©1994–2013, Quantachrome Instruments v11.03). The BET surface area was calculated by using the Brunauer-Emmett-Teller equation at the relative pressure (p/p_0) between 0.05 and 0.35 while the pore size distribution was obtained by the Barrett-Joyner-Halender (BJH) method. Before the analysis, samples were degassed at 120 °C for 3 h. The morphology of the samples was studied by a field emission scanning electron microscope (FE-SEM) (JSM-7600F Thermo NORAN System 7) while the functional groups analysis was conducted by Fourier transform infrared (FTIR) spectroscopy.

CDI measurements

The CDI performance of the prepared activated carbon was evaluated by using a two electrodes configuration, a working electrode (cathode) and a counter electrode (anode). The electrodes were prepared by mixing activated CF powder, carbon black, and polytetrafluoroethylene (PTFE) dispersion in H_2O suspensions 60 wt%, at a weight ratio of 8:1:1 in ethanol. The mixture was stirred for 2 h to ensure homogeneity and dried at 80 °C to form a dough-like paste, then the paste formed was rolled and cut into squares of size 3 cm × 3 cm, then dried at 50 °C for 12 h in the oven before testing to remove the remaining solvents.

Batch experiments were conducted to investigate the electrosorption of Pb^{2+} on the electrodes prepared from CF. The fabricated electrodes were placed in the CDI cell with $Pb(NO_3)_2$ solution, the volume of the solution was 30 mL and initial concentration $C_o = 100$ mg L^{-1}. Desalination experiments were performed with operating parameters of 1.2 V applied voltage, for 2 h cycle time for the adsorption stage by using potentiostat/galvanostat (Vertex.1A.EIS) (1A/10 V/1 MHz EIS, Ivium Technologies, The Netherlands, equipped with Iviumsoft electrochemistry software). The conductivity of the solution was continuously monitored by a conductivity meter (GMH 3400 series) after every 5 min. The Pb^{2+} solution concentrations were determined by using the calibration curve.

The removal of the Pb^{2+} ions by the CF activated carbon samples was characterized via removal efficiency (*RE*) and electrosorption capacity (*EC*) as shown in Equations (1) and (2):

$$RE = \frac{C_o - C_f}{C_o} \times 100\% \quad (1)$$

$$EC = \frac{(C_o - C_f)}{m} \times V \quad (2)$$

where C_o and C_f represent the initial and final concentrations (mg L^{-1}) of the Pb^{2+} ions, respectively; V is the total volume of solution (mL), and m is the mass of electrode material (g).

RESULTS AND DISCUSSION

Nitrogen adsorption isotherms of the samples

The textural properties of the CF samples, BET surface area (S_{BET}), micropore surface area (S_{micro}), mesopore surface area (S_{meso}), pore diameter (D_p), micropore volume (V_{micro}), mesopore volume (V_{meso}) and pore volume (V_p), are analyzed regarding the amount of KOH during activation as well as activation temperature and presented in Table 1.

The BET surface area of untreated carbon (CF-400) was approximately 642 $m^2 g^{-1}$ but increased to 1,642 $m^2 g^{-1}$ for CF-1-800-3 after activation with KOH at 800 °C. This increase in surface area can be attributed to KOH etching which creates more pores on the carbon materials. There was a further increase in surface area up to 2,481 $m^2 g^{-1}$ for the CF-4-800-3. These results show that the ratio KOH:CF also has an effect on surface area; a significant increase from 1,642 $m^2 g^{-1}$ for $R = 1$ (CF-1-800-3) to 2,481 $m^2 g^{-1}$ for $R = 4$ (CF-4-800-3) is observed while keeping the activation temperature constant at 800 °C. Furthermore, the surface area increases from 1,101 to 2,481 $m^2 g^{-1}$ as activation temperature rises at constant KOH to carbon impregnation ratio of 4. The pore size of all carbon samples ranges from 3.2 to 3.8 nm which is a clear indication of the mesopore type of the samples. Availability of mesopores should favor the electrosorption capacity of activated carbon as reported in the literature (Liu *et al.* 2013). From Table 1, one can see there is positive correlation between BET SSA and pore volume. Pore

Table 1 | Textual characteristics of CF activated carbon sample

Carbon sample	S_{BET} ($m^2\ g^{-1}$)	S_{micro} ($m^2\ g^{-1}$)	S_{meso} ($m^2\ g^{-1}$)	S_{micro}/S_{meso}	D_p (nm)	V_{micro} ($cm^3\ g^{-1}$)	V_{meso} ($cm^3\ g^{-1}$)	V_{micro}/V_{meso}	V_T ($cm^3\ g^{-1}$)
CF-400	642	230	412	0.56	3.3	0.06	0.47	0.13	0.53
CF-4-600-3	1,101	505	596	0.85	3.8	0.20	0.84	0.24	1.04
CF-4-700-3	1,666	814	852	0.96	3.5	0.30	1.17	0.26	1.47
CF-1-800-3	1,642	868	774	1.12	3.5	0.39	1.03	0.38	1.42
CF-2-800-3	1,808	646	1,162	0.56	3.4	0.34	1.21	0.28	1.55
CF-3-800-3	1,951	812	1,139	0.71	3.6	0.41	1.37	0.30	1.78
CF-4-800-3	2,481	972	1,509	0.64	3.2	0.49	1.49	0.33	1.98

volume increased with increasing activation temperature, as well as the amount of KOH. During activation, the increase in the amount of KOH to the sample is anticipated to widen the pores thus giving a larger pore volume resulting in increased surface area. Furthermore, a linear relationship between the total pore volume and the mesopore volume was observed. As the KOH:CF and activation temperature increase then the total pore volume and mesopore volume, respectively, increase. To further quantify porosity of the CF samples, the N_2 adsorption-desorption isotherms were determined; the effects of the KOH:CF ratio (Figure 1(a)) and activation temperature (Figure 1(b)) were investigated. One can see that the materials have both micropores and mesopores. The isotherms for the CF samples exhibit apparent hysteresis loops between the relative pressures of 0.4 and 0.8. According to the IUPAC classification, these curves exhibit type IV isotherms, showing that the materials are abundant with mesopores. It can be noted that all samples demonstrated a large amount of non-uniform mesopores as the absorbed N_2 volume keeps increasing significantly. Figure 2(a) and 2(b) show the pore size distribution as calculated using the BJH method. The plots depict that more pores were distributed at 4 nm which agrees well with the isotherms that indeed the samples have pores in the mesopores region. The presence of mesopores is very important for ions transfer, and they also act as an ion reservoir in the electrode.

Morphological analysis

To gain further insight into the morphology of CF samples, SEM micrographs were taken for the carbon activated at 1:1 and 4:1 KOH:CF ratios, as shown in Figure 3(a) and 3(b), respectively. Both SEM images exhibit irregular pore sizes; the flake-like and graphitic structure of the carbon with a rough surface is generated by KOH etching that brings this high porosity observed on the SEM micrographs which are paramount for CDI applications. Nevertheless at the higher ratio, 4:1, collapsed pores with few broken

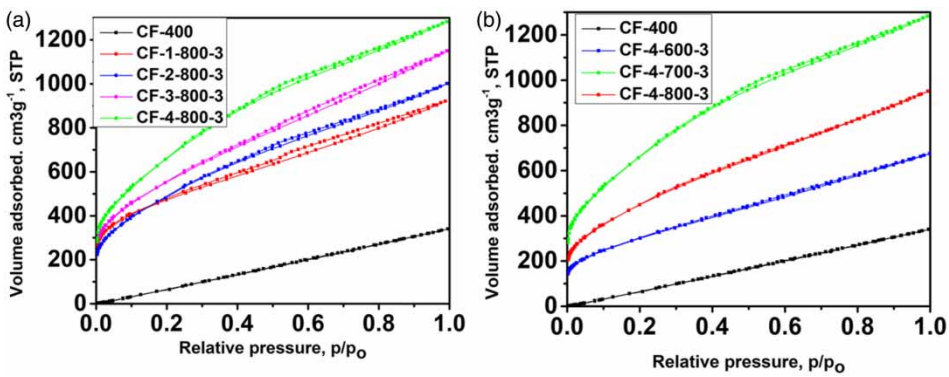

Figure 1 | Nitrogen adsorption-desorption isotherms of CF samples activated at (a) different KOH:CF ratios, $T_a = 800$ K, and (b) different activation temperatures, KOH:CF ratio 4:1.

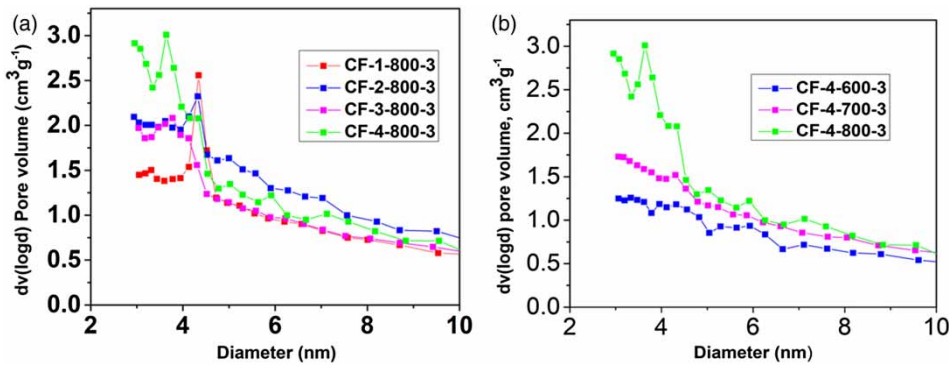

Figure 2 | Pore size distribution calculated from adsorption-desorption isotherms using BJH method for samples activated at (a) different KOH:CF ratios, $T_a = 800$ K, and (b) different activation temperatures, KOH:CF ratio 4:1.

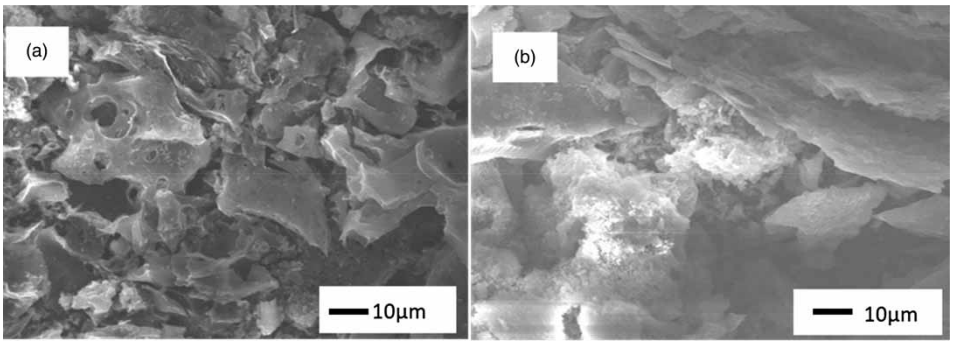

Figure 3 | SEM images for CF samples: (a) CF-1-800-3 and (b) CF-4-800-3.

channel-like structures can be seen (Figure 3(b)), which is in accordance with the decrease in pore volume observed for the same sample CF-4-800-3 mentioned above (Table 1).

FTIR analysis

FTIR analysis was used to identify the functional group present in the activated carbon surfaces. The FTIR spectra of the untreated carbon (CF-400) and activated samples were measured to compare the presence of surface chemical functional groups at various processing stages of CF (Figure 4). Peaks resulted at ~1,000 cm^{-1}, 1,700 cm^{-1}, and 2,200 cm^{-1} showing that, for untreated carbon, only bonds C-O, C = O and C ≡ C exist. These double and triple bonds might come from aromatic carbons in the chicken feather precursors. After activation with KOH, the new O-H and C-H bonds were introduced. The stretching vibrations of O-H, C-H and C-O were observed at 3,569–3,635 cm^{-1}, 2,904–2,939 cm^{-1}, and 1,041–1,191 cm^{-1}, respectively. The presence of a peak observed at ~1,550–1,700 cm^{-1} was assigned to C = C stretching vibrations. All activated carbon showed similar functional groups apparently because they were subjected to the same KOH chemical treatment. The oxygen-containing functional groups identified on the CF surfaces play a major role in metal sorption whereby during adsorption they bind with lead ions, hence improving the lead removal efficiency. The presence of hydroxyl and carbonyl functional groups enhances the wettability of the material which favors ionic adsorption during water treatment since it affects the total areas and ions removal rate.

Desalination experiments

The CDI electrosorption experiments were carried out with different CF electrodes to study the effects of activating agent to carbon ratio R and activating temperature T_a in CDI performance. The electrical conductivity of the

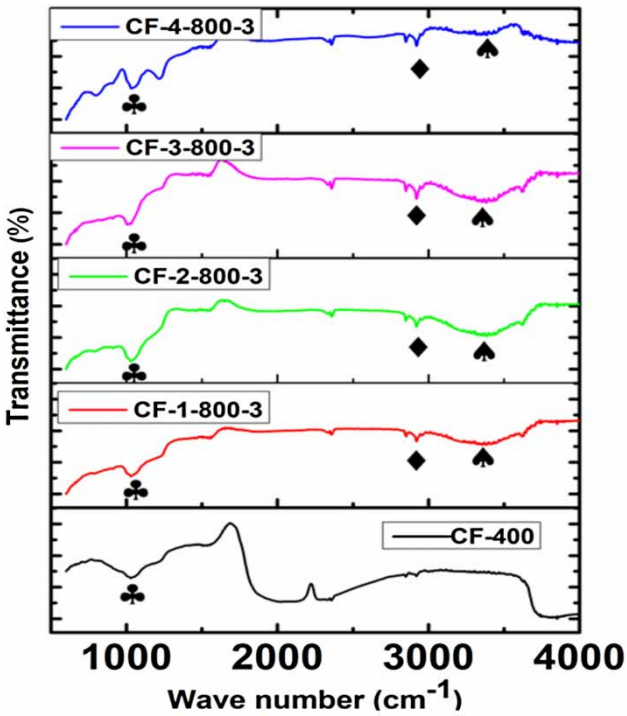

Figure 4 | FTIR spectra of the untreated carbon (CF-400) and CF activated samples; (♠) O-H, (♦) C-H, and (♣) C-O.

$Pb(NO_3)_2$ solution versus operating time was measured with untreated CF-400 and different activated CF electrodes; results are shown in Figure 5. The decrease in conductivity with time is observed for all CF electrodes, and saturation state is seen within less than 2 hours of the adsorption stage. The conductivity decreases from an initial value of 81.3 μS cm^{-1} to 19.7, 28.0, 31.4, and 35 μS cm^{-1} for CF-1-800-3, CF-2-800-3, CF-3-800-3, and CF-4-800-3 electrodes, respectively; hence the largest change occurs for the smallest KOH:CF ratio, $R = 1$ (Figure 5(a)). Increase in activation temperature T_a of the CF samples results in more effectual desalination (Figure 5(b)) as final conductivity of the $Pb(NO_3)_2$ solution drops from 69 μS cm^{-1} ($T_a = 600$ K) to 35 μS cm^{-1} ($T_a = 800$ K). At the same time, practically no change in conductivity is seen for the sample CF-400 prepared without KOH treatment.

The lead removal efficiencies of CF samples calculated by Equation (1), are represented in the bar diagrams (Figure 6). The CF-1-800-3 electrode displays higher removal efficiency (81%) toward Pb^{2+} compared with the other electrodes as shown in Figure 6(a). These results indicate that as the activating agent to carbon ratio increases, the removal efficiency decreases, irrespective of the increased BET surface area (Table 1). This may be due to the etching phenomenon of activating agent KOH which distorts the pores as the amount increases. Thus, the active surface for adsorption of the ions becomes smaller than the BET surface area. Therefore, efforts to make electrodes with high surface areas are still not so important as removal efficiency depends on other factors as opined, for example, by Seo *et al.* (2010). Figure 6(b) shows the behavior of electrodes with CF-4-T_a-3 samples prepared at different activation temperatures: the CF-4-800-3 exhibits higher removal efficiency (61%) of Pb^{2+} than the other samples. These results show that the removal efficiency increases with an increase in activation temperature. This is due to the fact that as activation temperature increases

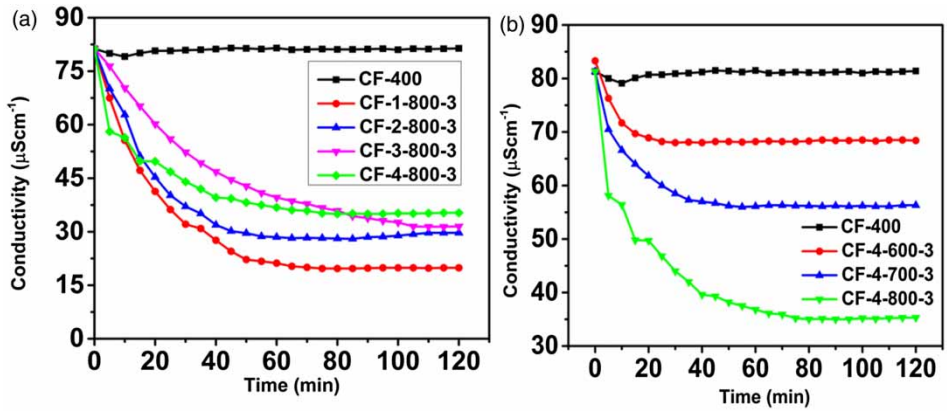

Figure 5 | Desalination experiment with the CF carbon electrodes at different (a) KOH:CF ratios and (b) activation temperatures.

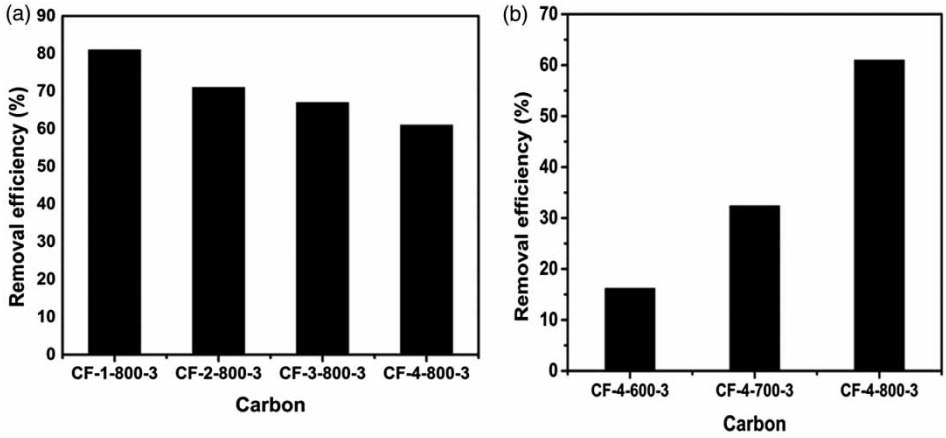

Figure 6 | Lead removal efficiency of CF electrodes: (a) effect of KOH:CF ratio; (b) effect of activating temperature.

the surface area also increases as proved by BET results (Table 1), thus increasing the adsorption sites.

The electrosorption capacities *EC* of the CF samples calculated by Equation (2) are presented in Figure 7(a) and 7(b). The electrode prepared with the CF-1-800-3 exhibits maximum $EC = 4.1\ \mathrm{mg \cdot g^{-1}}$ on the removal of the Pb^{2+} ions which is in agreement with the highest removal efficiency for the same sample (Figure 6(a)) as well as highest desalination efficacy (Figure 5(a)). It is worth noting that the sample with maximum electrosorption capacity, CF-1-800-3, does not possess the largest surface area as shown in Table 1. It seems that an increase in the amount of activating agent might result in enlarging the specific surface area of the sample but not always result in the best adsorptivity. Therefore no direct accordance is observed between the BET surface area and the electrosorption capacity of samples. This is also observed by Wang *et al.* (2010).

General discussion of the results

The effect of activating temperature on the CF samples is summarized in Table 2. The results show a direct relationship between activation temperatures and BET surface area; the BET surface area increases as activation temperature increases; this result is supported by Zhao *et al.* (2015). Also, it was observed that the electrode materials with high BET surface area exhibit high removal efficiency as well as electrosorption capacity.

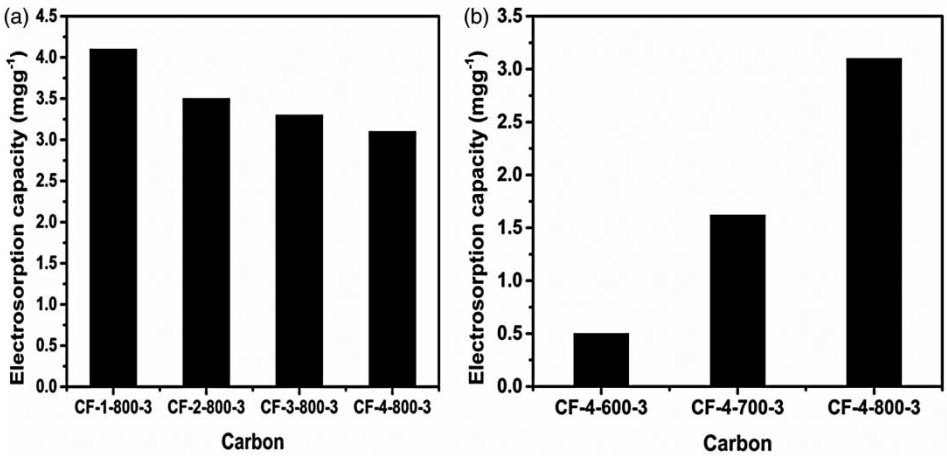

Figure 7 | Electrosorption capacity of lead by CF electrodes: (a) effect of KOH:CF ratio; (b) effect of activating temperature.

Table 2 | Relationship between the CF-4-T_a-3 samples textural properties and adsorption performance of the electrodes: effect of activating temperature T_a

T_a (°C)	S_{BET} ($m^2\ g^{-1}$)	D_{BJH} (nm)	V_P ($cm^3\ g^{-1}$)	RE (%)	EC ($mg\ g^{-1}$)
600	1,101	3.8	1.04	16.2	0.5
700	1,666	3.5	1.47	32.4	1.6
800	2,481	3.2	1.98	61	3.1

Table 3 | Relationship between the CF-*R*-800-3 samples textural properties and adsorption performance of the electrodes: effect of the KOH:CF ratio (*R*)

R	S_{BET} ($m^2\ g^{-1}$)	D_{BJH} (nm)	V_P ($cm^3\ g^{-1}$)	RE (%)	EC ($mg\ g^{-1}$)
1	1,642	3.5	1.42	81	4.1
2	1,808	3.4	1.55	71	3.5
3	1,951	3.6	1.78	67	3.3
4	2,481	3.2	1.98	61	3.1

The results summarized in Table 3 show the effect of activating agent ratio on the CF samples; the results revealed that there is a linear relationship between the activating agent ratio and the BET surface area. The surface area is increasing with the increase in the amount of KOH. During activation, the increase in the amount of KOH to the sample is anticipated to widen the pores thus giving a larger pore volume and increasing the surface area, as supported by Enock *et al.* (2017). However, the higher the ratio *R*, the larger the surface area, but the lower the sorption ability. This means in CDI the high surface area is not the only factor that contributes to the good electrosorption capability of the electrode materials. It depends on other factors such as the number of electrosorption sites and electrical double layer (EDL) overlapping effect; this means that for good electrosorption capacity there should be a balance between the number of electrosorption sites and EDL overlapping effect. Moreover, pore size and structure of the electrodes enhances the removal efficiency; so, if the pore size of the hydrated ion is compatible with the size of the pores of the sample then adsorption of the ions could be improved (Largeot *et al.* 2008). Furthermore, appropriate pore size distribution between micropore and mesopore is required to improve the CDI performance as supported by Seo *et al.* (2010) and Wang *et al.* (2010).

Recent CDI electrode materials present in the literature for the removal of Pb^{2+} are summarized in Table 4. The Pb^{2+} removal efficiency of the activated carbon cloth electrode under a cell voltage of 1.2 was 43% (Huang *et al.* 2016), for the 3D graphene-based asymmetric electrode with a mass of 100 mg the removal efficiency of Pb^{2+} reached 99.9% (Liu *et al.* 2017). Fe_3O_4/porous graphene

Table 4 | Comparison of the CF and other materials for lead removal from water used in CDI

Material	RE (%)	EC ($mg\ g^{-1}$)	C_0 ($mg\ L^{-1}$)	*V* (V)	Time (min)	Volume (mL)	Flow rate ($mL\ min^{-1}$)	Approach/ Mode	Size of electrodes	Reference
AC cloth	43	17.8	165.6	1.2	120	60	0	Batch	1 inch × 1 inch	Huang *et al.* (2016)
3D graphene	99.9	6.99	20	1.4	60	35	40	Batch	115 mm × 7 mm × 1 mm	Liu *et al.* (2017)
AC with ion-exchange membrane	80	0.18	1	1.2	60	1,000	23	Single-pass	4.2 inch × 4.2 inch	Dong *et al.* (2018)
Carbon nanotube (activated by air plasma)	*	3.40	10	0.45	5	200	4	Batch	30 mm × 50 mm	Yang *et al.* (2014)
Fe_3O_4/porous graphene nanocomposite	90	47	9.9	1.2	5	150	4	Batch	80 mm × 30 mm × 0.3 mm	Bharath *et al.* (2017)
O-doped BN nanosheet	*	220	600	1.2	20	100	50	Batch mode	2 cm × 2 cm	Chen *et al.* (2017a, 2017b)
CF	81	4.1	100	1.2	120	30	5	Batch mode	3 cm × 3 cm	This study

Note: * data not found; AC, activated carbon; RE, removal efficiency; EC, electrosorption capacity; BN, boron nitride.

nanocomposite electrode was used and the efficiency removal of Pb^{2+} reached 90% under a constant voltage of 1.2 V (Bharath *et al.* 2017). Also activated carbon with an ion-exchange membrane was investigated for Pb^{2+} removal and the removal efficiency was 80%. Graphene electrodes exhibit the highest removal efficiency of Pb^{2+}, but the high price and high manufacturing cost limit graphene for practical use as an ideal electrode material in CDI technology. Hence activated carbon derived from abundant, low-cost and environmentally friendly chicken feathers exhibited comparable electrosorption capacity as well as removal efficiency of lead ions from water by CDI technology.

CONCLUSION

In this study, the capacitive deionization performances for Pb^{2+} removal from dilute aqueous $Pb(NO_3)_2$ solutions using electrodes derived from chicken feathers were investigated.

The CF-4-800-3 exhibited good lead removal efficiency of 81% from aqueous solution and an electrosorption capacity of 4.1 mg g^{-1}. Moreover, experimental results revealed that the effect of activating agent ratio does not prove a direct relationship between the removal efficiency and BET surface area, which is the opposite to the effect of activation temperature. Electrosorption capacity and removal efficiency do not depend on only BET surface area; rather other factors need to be considered. Generally, the results of this work show that electrode materials derived from chicken feathers can be suitable for removing heavy metals such as Pb^{2+} from aqueous solution using the CDI technique.

ACKNOWLEDGEMENTS

The authors acknowledge the World Academy of Sciences (TWAS, grant number: 16-529 RG/CHE/AF/AC_G – FR3240293305 dated 12 December 2016) and Water Infrastructure and Sustainable Energy Futures (WISE–Futures) African Center of Excellence for financial support.

REFERENCES

Baroud, T. N. & Giannelis, E. P. 2018 High salt capacity and high removal rate capacitive deionization enabled by hierarchical porous carbons. *Carbon* **139**, 614–625. doi:10.1016/j.carbon.2018.05.053.

Bharath, G., Alhseinat, E., Ponpandian, N., Khan, M. A., Siddiqui, M. R., Ahmed, F. & Alsharaeh, E. H. 2017 Development of adsorption and electrosorption techniques for removal of organic and inorganic pollutants from wastewater using novel magnetite/porous graphene-based nanocomposites. *Separation and Purification Technology* **188**, 206–218.

Chen, F., Huang, Y., Guo, L., Ding, M. & Yang, H. Y. 2017a A dual-ion electrochemistry deionization system based on AgCl-Na0.44MnO2 electrodes. *Nanoscale* **9** (28), 10101–10108. doi:10.1039/c7nr01861d.

Chen, M. M., Wei, D., Chu, W., Wang, T. & Tong, D. G. 2017b One-pot synthesis of O-doped BN nanosheets as a capacitive deionization electrode for efficient removal of heavy metal ions from water. *Journal of Materials Chemistry A* **5** (32), 17029–17039. doi:10.1039/C7TA05459A.

de la Rosa, G., Reynel-Avila, H. E., Bonilla-Petriciolet, A., Cano-Rodriguez, I., Velasco-Santos, C. & Martínez-Hernández, A. 2008 Recycling poultry feathers for Pb removal from wastewater: kinetic and equilibrium studies. *International Journal of Chemical and Biomolecular Engineering* **1** (4), 185–193.

Dong, Q., Guo, X., Huang, X., Liu, L., Tallon, R., Taylor, B. & Chen, J. 2018 Selective removal of lead ions through capacitive deionization: role of ion-exchange membrane. *Chemical Engineering Journal*. doi:10.1016/j.cej.2018.10.208.

Enock, T. K., King'ondu, C. K., Pogrebnoi, A. & Jande, Y. A. C. 2017 Biogas-slurry derived mesoporous carbon for supercapacitor applications. *Materials Today Energy* **5**, 126–137.

Huang, Z., Lu, L., Cai, Z. & Ren, Z. J. 2016 Individual and competitive removal of heavy metals using capacitive deionization. *Journal of Hazardous Materials* **302**, 323–331.

Jande, Y. A. C. 2015 *Modeling and Application of Capacitive Deionization in Desalination and CO_2 Capture*. PhD thesis, Mechanical Engineering, Hanyang University Graduate School, Seoul, Republic of Korea.

Lado, J. J., Zornitta, R. L., Calvi, F. A., Tejedor-Tejedor, M. I., Anderson, M. A. & Ruotolo, L. A. 2016 Study of sugar cane bagasse fly ash as electrode material for capacitive deionization. *Journal of Analytical and Applied Pyrolysis* **120**, 389–398.

Largeot, C., Portet, C., Chmiola, J., Taberna, P.-L., Gogotsi, Y. & Simon, P. 2008 Relation between the ion size and pore size for an electric double-layer capacitor. *Journal of the American Chemical Society* **130** (9), 2730–2731.

Li, N., An, J., Wang, X., Wang, H., Lu, L. & Ren, Z. J. 2017 Resin-enhanced rolling activated carbon electrode for efficient

capacitive deionization. *Desalination* **419**, 20–28. doi:10.1016/j.desal.2017.05.035.

Liu, Y., Li, H., Nie, C., Pan, L. & Sun, Z. 2013 Carbon nanotube and carbon nanofiber composite films grown on different graphite substrate for capacitive deionization. *Desalination and Water Treatment* **51** (19–21), 3988–3994. doi:10.1080/19443994.2013.795020.

Liu, P., Yan, T., Zhang, J., Shi, L. & Zhang, D. 2017 Separation and recovery of heavy metal ions and salt ions from wastewater by 3D graphene-based asymmetric electrodes via capacitive deionization. *Journal of Materials Chemistry A* **5** (28), 14748–14757. doi:10.1039/c7ta03515b.

Machunda, R., Jeon, H., Lee, J. & Lee, J. 2009 Effects of acid treatment on the improvement of specific capacitance and deionization efficiency of porous carbon electrodes. *Water Science & Technology: Water Supply* **9** (2), 159–165.

Mdegela, R. H., Braathen, M., Pereka, A. E., Mosha, R. D., Sandvik, M. & Skaare, J. U. 2009 Heavy metals and organochlorine residues in water, sediments, and fish in aquatic ecosystems in urban and peri-urban areas in Tanzania. *Water, Air, and Soil Pollution* **203** (1–4), 369–379.

Peng, Q., Liu, L., Luo, Y., Zhang, Y., Tan, W., Liu, F., Suib, S. L. & Qiu, G. 2016 Cadmium removal from aqueous solution by a deionization supercapacitor with a birnessite electrode. *ACS Applied Materials & Interfaces* **8** (50), 34405–34413.

Porada, S., Weinstein, L., Dash, R., van der Wal, A., Bryjak, M., Gogotsi, Y. & Biesheuvel, P. M. 2012 Water desalination using capacitive deionization with microporous carbon electrodes. *ACS Applied Materials & Interfaces* **4** (3), 1194–1199. doi:10.1021/am201683j.

Prasanthi, N., Bhargavi, S. & Machiraju, P. 2016 Chicken feather waste: a threat to the environment. *International Journal of Innovative Research in Science and Technology* **5** (9), 16759–16764.

Seo, S. J., Jeon, H., Lee, J. K., Kim, G. Y., Park, D., Nojima, H., Lee, J. & Moon, S. H. 2010 Investigation on removal of hardness ions by capacitive deionization (CDI) for water softening applications. *Water Research* **44** (7), 2267–2275. doi:10.1016/j.watres.2009.10.020.

Suss, M. E., Porada, S., Sun, X., Biesheuvel, P. M., Yoon, J. & Presser, V. 2015 Water desalination via capacitive deionization: what is it and what can we expect from it? *Energy & Environmental Science* **8** (8), 2296–2319. doi:10.1039/c5ee00519a.

Wang, M., Huang, Z.-H., Wang, L. & Kang, F. 2010 Electrochemical Capacitive Desalination Behavior of Activated Carbon Fibers. Retrieved from https://pdfs.semanticscholar.org/5942/f37461e82e3fc570be379ca468e995411f3d.pdf.

Wang, Q., Cao, Q., Wang, X., Jing, B., Kuang, H. & Zhou, L. 2013 A high-capacity carbon prepared from renewable chicken feather biopolymer for supercapacitors. *Journal of Power Sources* **225**, 101–107. doi:10.1016/j.jpowsour.2012.10.022.

Yang, L., Shi, Z. & Yang, W. 2014 Characterization of air plasma-activated carbon nanotube electrodes for the removal of lead ion. *Water Science and Technology* **69** (11), 2272–2278.

Yang, C., Liu, Y., Ma, C., Norton, M. & Qiao, J. 2015 Preparing desirable activated carbons from agricultural residues for potential uses in water treatment. *Waste and Biomass Valorization* **6** (6), 1029–1036. doi:10.1007/s12649-015-9408-x.

Zhao, Z., Wang, Y., Li, M. & Yang, R. 2015 High performance N-doped porous activated carbon based on chicken feather for supercapacitors and CO_2 capture. *RSC Advances* **5** (44), 34803–34811. doi:10.1039/c5ra01569c.

First received 23 December 2018; accepted in revised form 14 March 2019. Available online 22 April 2019